Linear and nonlinear optical properties of the piezoelectric crystal α-GeO 2

Théodore Remark, P. Segonds, Alexandra Pena Revellez, Bertrand Menaert, Jérôme Debray, David Jegouso, Maria Cinta Pujol, Benoît Boulanger

Research Article | Vol. 11, No. 10 / 1 Oct 2021 / Optical Materials Express 3520
Optical Materials EXPRESS

Linear and nonlinear optical properties of the piezoelectric crystal α-GeO_2

THÉODORE REMARK,[1] PATRICIA SEGONDS,[1,3] ALEXANDRA PEÑA,[1] BERTRAND MENAERT,[1] JÉRÔME DEBRAY,[1] DAVID JEGOUSO,[1] MARIA CINTA PUJOL,[2] AND BENOÎT BOULANGER[1,4]

[1] *Univ. Grenoble Alpes, CNRS, Grenoble INP, Institut Néel, F-38000 Grenoble, France*
[2] *Univ. Rovira and Virgili, Dept Quim Fis and Inorgan, Fis and Cristallog Mat and Nanomat FiCMA FiCNA EMaS, Campus Sescelades, E-43007, Tarragona, Spain*
[3] *patricia.segonds@neel.cnrs.fr*
[4] *benoit.boulanger@neel.cnrs.fr*

Abstract: We report the first measurements of phase-matching angles for second-harmonic generation, sum- and difference- frequency generations performed over the transparency range of the uniaxial α-GeO_2 crystal. A simultaneous fit of these data provided dispersion equations. The optical damage threshold and the magnitude of the nonlinear coefficient d_{11} are also determined. We found $|d_{11}^{GeO2}(0.67\ \mu\text{m})| = 0.76\ \pm 0.09$ pm/V.

1. Introduction

There is still a great interest of finding new nonlinear crystals able to generate an optical parametric coherent radiation in the 3 - 5 µm band of transmission of the atmosphere. We identified α-GeO_2 as a serious candidate. This crystal is well known for its piezoelectric properties at high temperatures [1]. It crystallizes in the trigonal crystal class 32 with the space group $P3_121$ or $P3_221$, thus being iso-structural to the SiO_2 α-Quartz [2]. Then from the optical properties, it belongs to the uniaxial optical class, which potentially allows birefringence phase-matching to be achieved [3]. In point group 32 and using the contracted notation, there are 5 non-zero coefficients of the second-order electric susceptibility tensor that reduce to only 3 coefficients linked by the following equalities under Kleinman's assumption: $d_{11} = -d_{12} = -d_{26}$ [3].

Linear optical properties of α-GeO_2 crystals grown by a hydrothermal method had been investigated in the dielectric frame (x, y, z) [4]. Note that this orthonormal frame does not correspond to the crystallographic frame (**a**, **b**, **c**) where (**a**, **b**) = 120 °: the **c**-axis is collinear to z-axis, while the **a**-axis and **b**-axis are collinear to the x-axis, the y-axis being perpendicular to the x-axis. Then the (x,y) plane and (**a**, **b**) plane are coplanar. The optical transmission range was found between 0.21 µm and 6.5 µm using unpolarized light, with a maximal transmission coefficient of 80% in the visible range, and an absorption peak around 3 µm, due to incorporation of OH^- ions into the crystal. It was accompanied with several others between 5 µm and 6.5 µm [4,5]. Using the prism method, the ordinary and extraordinary principal refractive indices were measured at four wavelengths of the visible range, *i.e.* 0.436, 0.546, 0.578 and 0.632 µm, with a relative precision of the order of one percent. These data have shown that α-GeO_2 is a positive uniaxial crystal since $n_o(\lambda) < n_e(\lambda)$, and their fit provided preliminary dispersion equations, *i.e.* $n_{o,e}^2(\lambda) = 1 + B_{o,e}\lambda^2(\lambda^2 - C^2)^{-1}$ where C= 0.208 µm, $B_o = 1.64$ and $B_e = 1.76$, the subscripts *o* and *e* standing for the ordinary and extraordinary refractive indices respectively [4]. Recent calculations using the density functional theory (DFT) led to the prediction of the magnitude and sign of the unique non-zero nonlinear tensor coefficient, *i.e.* $d_{11} \simeq -1.5$ pm/V [6].

In the present paper, we report for the first time, to the best of our knowledge, direct measurements of phase-matching conditions for different nonlinear second-order frequency conversion processes. We used a α-GeO_2 crystal shaped as a cylinder in order to access any

#439099 https://doi.org/10.1364/OME.439099
Journal © 2021 Received 29 Jul 2021; revised 9 Sep 2021; accepted 9 Sep 2021; published 24 Sep 2021

Optical Materials EXPRESS

propagation direction in the plane of interest. The fit of all our data allowed us to obtain reliable dispersion equations of the ordinary and extraordinary principal refractive indices of this crystal. The magnitude of the unique nonlinear coefficient d_{11} of α-GeO_2 as well as the energy and intensity threshold damage in the picosecond and nanosecond regimes were also determined relatively to KTP by using oriented slabs.

2. Transparency range and optical damage threshold

We studied millimeter-size α-GeO_2 crystals of very good quality, grown by the Top Seeded Solution Growth (TSSG) method showing a high thermal stability [1,5].

Transmission spectra have been recorded in polarized light through a 0.78 mm-thick α-GeO_2 y-axis slab-oriented by X-rays SECASI goniometer working in θ−2θ configuration. The two faces perpendicular to the y-axis are polished to optical quality and uncoated; the slab is shown in inset of Fig. 1. We used a Perkin-Elmer Lambda 900 spectrometer running from 0.2 µm to 3.0 µm, and a Bruker FT-IR in the 3–7 µm range. The linear polarization of the input beam was controlled and oriented using a Glan Taylor polarizer. The recorded spectra without correction of Fresnel losses are given in Fig. 1. It shows that the transmission of α-GeO_2 increases continuously from an ultra-violet edge below 0.22 µm that is highlighted in inset of Fig. 1. The transmission reaches up to 80% from 1 µm before decreasing from 4.5 µm down to zero at 6.3 µm corresponding to the infrared cutoff. Several absorption peaks are located between 5 µm and 6.5 µm, but nothing near 3 µm thanks to our growth method that prevents any incorporation of OH^- ions into the crystal.

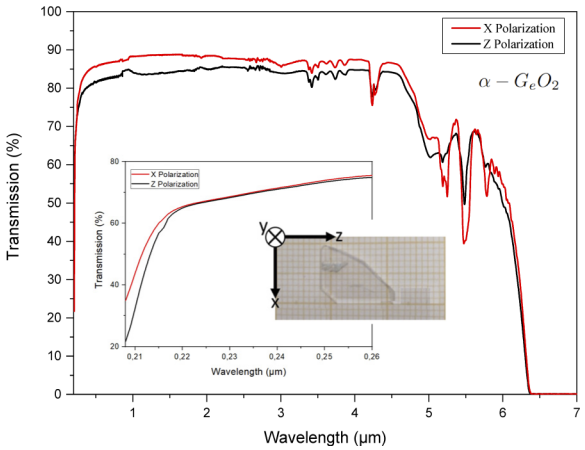

Fig. 1. : α-GeO_2 transmission spectra in polarized light recorded through a 0.78-mm-thick y-cut uncoated slab. The inset is a zoom of the Ultra-Violet edge. The picture shows the slab that was used for recording data.

Optical damage threshold was determined at λ=1.064 µm using a 0.47-mm-thick α-GeO_2 slab. It was cut oriented along the direction (θ = 57.6°, φ = 90°), where θ and φ are the angles of spherical coordinates in the dielectric frame. The sample was polished to optical quality and uncoated. The nanosecond and picosecond regimes were considered thanks to two linearly polarized Nd:YAG lasers emitting FWHM pulse widths of τ^{nano} = 10 ns and τ^{pico} = 15 ps with a repetition rate of 10 Hz. Their energy was varied by inserting a half-wave plate followed by a Glan Taylor polarizer before the crystal, and it was controlled by a pyroelectric Ophir PE10 Joulemeter over an average of 500 pulses.

The incident beam was focused at normal incidence at the entrance surface of the α-GeO_2 slab by using a lens with a focal length ensuring a Rayleigh length greater than the sample thickness, and the resulting beam waist *radius* was determined by using the knife method.

Optical Materials EXPRESS

In the nanosecond regime, a focal length f ^{nano} of 200 mm provided a beam waist *radius* $w_o^{nano} = 60 \pm 5$ µm and a corresponding Rayleigh length $Z_R^{nano} = 11 \pm 2$ mm. In the picosecond regime, we had f^{pico} = 400 mm leading to $w_o^{pico} = 97 \pm 5$ µm and $Z_R^{pico} = 28 \pm 3$ mm.

The optical damage threshold was observed using a CCD camera, the goal being to detect early stage damage at the entrance surface of the slab after a continuous exposure to the laser beam for one minute at fixed energy. Between two exposures on the same area of the slab, the energy was continuously increased from 0 J in 250 µJ steps in the nanosecond regime, whereas 25 µJ steps were required in the picosecond regime. By increasing the energy step by step, we finally observed a damage on our slab. Then, the same protocol was repeated on a new area of the same slab starting from 0 J. We reproduced this protocol 5 times, in 5 different spots of the sample, and found an optical damage threshold $E_{GeO2}^{nano} = 1853 \pm 5$ µJ corresponding to a peak power density $P_{GeO2}^{nano} = 2.6 \pm 0.4$ GW/cm^2 in the nanosecond regime. It was reduced down to $E_{GeO2}^{pico} = 125 \pm 5$ µJ in the picosecond regime leading to $P_{GeO2}^{pico} = 45 \pm 6$ GW/cm^2. For comparison, we studied under the same conditions a 0.26-mm-thick KTP slab cut oriented at ($\theta = 58.5°$, $\varphi = 90°$) from Cristal Laser SA: we found $E_{KTP}^{nano} = 1515 \pm 5$ µJ ($P_{KTP}^{nano} = 2.1 \pm 0.4$ GW/cm^2) in the nanosecond regime and $E_{KTP}^{pico} = 154 \pm 5$ µJ ($P_{KTP}^{pico} = 55 \pm 7$ GW/cm^2) in the picosecond one. Thus, the optical damage threshold of α-GeO_2 and KTP are of the same order of magnitude.

3. Phase-matching conditions and dispersion equations

Regarding the crystal class of α-GeO_2, the following interactions can be investigated under phase-matching conditions with an associated non-zero effective coefficient in the (y, z) plane, *i.e.* Type I Sum-Frequency Generation (SFG : $1/\lambda_3^o = 1/\lambda_1^e + 1/\lambda_2^e$), Type I Second-Harmonic Generation (SHG : $1/\lambda_{2\omega}^o = 1/\lambda_\omega^e + 1/\lambda_\omega^e$) and Type II Difference-Frequency generation (DFG : $1/\lambda_1^e = 1/\lambda_3^o - 1/\lambda_2^e$), with $\lambda_1 \geq \lambda_2 > \lambda_3$ and where *o* and *e* stand for the ordinary and the extraordinary polarizations respectively. Note that for SFG, λ_1 and λ_2 are the incoming wavelengths and λ_3 is generated one; in the case of SHG, it comes $\lambda_1 = \lambda_2 = \lambda_\omega$ and $\lambda_3 = \lambda_{2\omega} = \lambda_\omega/2$. For DFG, the incident wavelengths are λ_2 and λ_3, λ_1 being the generated one. Their phase-matching *loci* were directly determined in a α-GeO_2 crystal shaped as a cylinder, with the curved face polished to optical quality and a diameter of D = 9.17 ± 0.1 mm, the acylindricity accuracy ΔD/D being of about 1% [7]. It is shown in inset of Fig. 2 where the bias face and the two black lines correspond respectively to a natural face and to the best volume of the crystal. The revolution axis of the cylinder was oriented collinear with the x-axis, with an accuracy better than 0.5° by using an X-Rays backscattered Laue method. Thus the (y, z) plane of interest can be scanned by rotating the cylinder on it-self when stuck on a goniometric head and placed at the center of an automatic Kappa circle. We already used this cylinder shape for the characterization of the nonlinear optical properties of other nonlinear crystals as BNA for example [8].

In the present case, we used different input beams emitted by a 15-ps-FWHM pulse duration and 10-Hz-repetition rate Light Conversion source that is tunable from 2.0 µm to 11.0 µm. The first stage is an Optical Parametric Generator (OPG) tunable between 0.4 µm and 2.2 µm that is pumped by the Third-Harmonic of a 1.064 µm Leopard Nd:YAG laser from Excel Technology. The second stage is based on a $AgGaS_2$ Difference-Frequency-Generator ($AgGaS_2$-DFG) pumped by both the OPG and part of the 1.064 µm beam. The pulsed source also provides a beam at 0.532 µm generated by the Second-Harmonic of 1.064 µm. Achromatic half wave-plates allowed us to adjust the orientation of the linear polarization of all these beams independently, and their energy was controlled by using an OPHIR PE10 Joulemeter.

The fundamental wavelength used for SHG was provided by the OPG up to 2.2 µm and by the $AgGaS_2$-DFG up to the 6.5 µm, which corresponds to the Infrared cut-off of α-GeO_2. For SFG and DFG, the OPG beam and part of the 1.064 µm Nd:YAG beam were collinearly combined directly in the cylinder. We also used the 0.532 µm beam for SFG studies. The parallel

Optical Materials EXPRESS

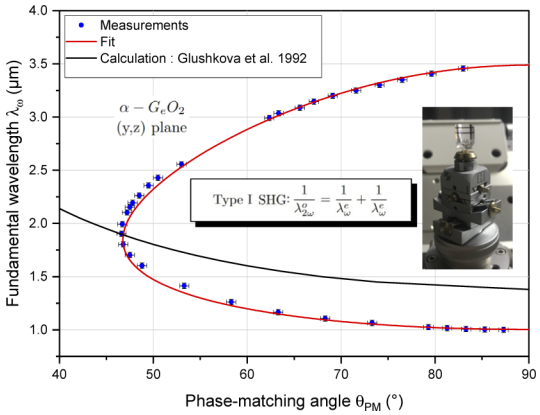

Fig. 2. Type I SHG turning curve in the (y, z) plane of the α-GeO_2. The measurements were performed using the α-GeO_2 cylinder shown in inset. The exponents "o" and "e" denote the ordinary and extraordinary polarizations, respectively.

propagation along the diameter of the α-GeO_2 cylinder of all incoming beams was insured for any orientation by using a 100-mm-focal length CaF_2 lens. The phase-matching angles θ_{PM} were directly read on the Kappa circle with an accuracy of ± 0.5 °.They correspond to the optima of energy conversion efficiency of SHG, SFG or DFG at the generated wavelengths. All wavelengths were controlled with an accuracy of ± 2 nm. We used three detectors: 650 Red Tide IDIL spectrometer below 1.1 µm, NIRquest 512 Ocean Optics spectrometer up to 1.7 µm, and Vigo infrared photoelectromagnetic detector (PEM) between 1 µm and 3 µm. Figures 2, 3 and 4 show the tuning curves obtained in the (y, z) plane of α-GeO_2 . In Fig. 2, corresponding to type I SHG, the fundamental wavelength λ^e_ω is given as a function of phase-matching angle θ_{PM}.

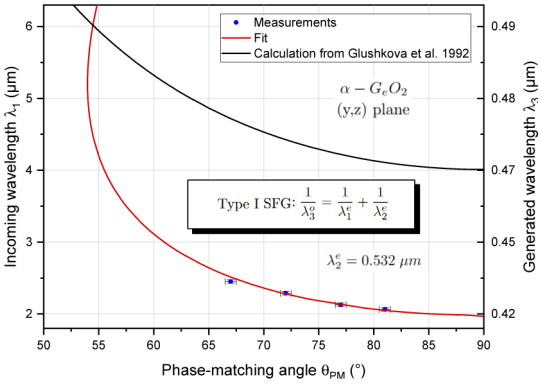

Fig. 3. Type I SFG in the (y, z) plane of α-GeO_2. The exponents "o" and "e" denote the ordinary and extraordinary polarizations, respectively.

The tuning curve of Type I SFG is shown in Fig. 3: λ^e_1 is the tunable incoming wavelength and λ^e_2 = 0.532 µm. In Fig. 4, λ^e_2 = 1.064 µm is one of the two incoming wavelengths: the lower part of the tuning curve corresponds to Type I SFG, where the other incoming wavelength λ^e_1 is below 2.5 µm and λ^o_3 is generated; the upper part describes Type II DFG, where λ^o_3 is the other incoming wavelength and λ^e_1 is generated. According to Fig. 4, it appears that birefringence phase-matching is allowed up to the infrared cutoff of α-GeO_2.

Optical Materials EXPRESS

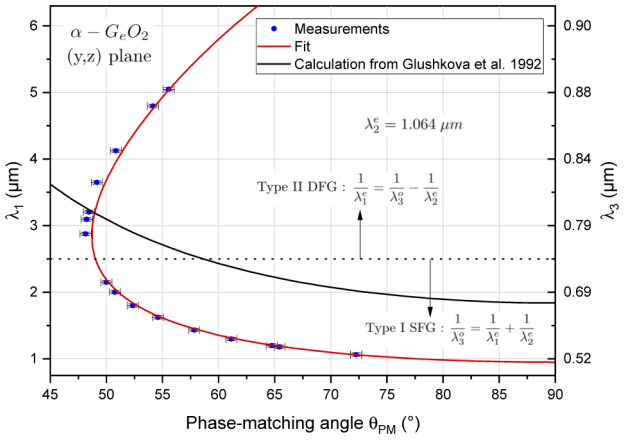

Fig. 4. Type I SFG and Type II DFG in the (y, z) plane of α-GeO_2. The exponents "o" and "e" denote the ordinary and extraordinary polarizations, respectively.

All our experimental data are in strong disagreement with the tuning curves calculated from the dispersion equations of Ref. [4]. We think that such a difference cannot be due to the growth technique, *i.e.* hydrothermal versus flux, but from the measurement it-self. Actually, in Ref. [4], the ordinary and extraordinary principal refractive indices were measured only at a few numbers of close wavelengths, *i.e.* 0.436, 0.546, 0.578 and 0.632 µm, on the one hand, and with a relative accuracy $\Delta n/n \approx 10^{-2}$ on the other hand. It is then impossible on this basis to perform a reliable calculation of phase-matching curve. At the opposite in our case, the refractive indices were determined from phase-matching data that are well spread in the transparency range and measured with an accuracy of ± 0.5°, which leads to a precision of better than 10^{-4}. In these conditions, it is then possible to calculate any phase-matching curve with an accuracy of ± 0.5°. Using an Levenberg-Marquardt algorithm encoded with Python, a simultaneous fit of all our measured phase-matching curves led to the determination of reliable dispersion equations of α-GeO_2 over its full transparency range. We also need the absolute magnitude of n_o and n_e at a given wavelength in order to fix the absolute magnitude of the dispersion equations: we took $n_o(\lambda = 0.6328\ \mu m) = 1.69550 \pm 4 \times 10^{-5}$ and $n_e(\lambda = 0.6328\ \mu m) = 1.72217 \pm 4 \times 10^{-5}$ determined by using a commercial refractometer Prism coupler Metricon.

Among different possible forms of equations, the best result was obtained with the following one:

$$n_i^2(\lambda) = A_i + \frac{B_i}{\lambda^2 - C_i} - D_i\lambda^2 \tag{1}$$

where λ is in µm and "i" stands to "o" and "e". The corresponding fitting parameters A_i, B_i, C_i and D_i are summarized in Table 1. The relative accuracy $\Delta n_i/n_i$ is better than 10^{-4}.

Table 1. Dispersion coefficients for the two principal refractive indices n_o and n_e of α-GeO_2.

Dispersion coefficients	A_i	B_i	C_i	D_i
i ≡ o	2.7970	0.0329	0.0005	0.0113
i ≡ e	2.9152	0.0197	0.0860	0.0119

The red continuous lines in Figs. 2 to 4 correspond to the phase-matching curves calculated with Eq. (1) and the coefficients of Table 1. According to the spectral range of our measurements, the description of the ordinary principal refractive index $n_o(\lambda)$ by Eq. (1) is valid from 0.42 µm to 1.73 µm, while it is from 0.532 µm to 5.05 µm for the extraordinary principal refractive n_e (λ).

Optical Materials EXPRESS

4. Nonlinear coefficient

The following step was to determine the magnitude of d_{11} that is the single nonlinear coefficient of α-GeO_2. According to Fig. 2, it can be obtained under type I-SHG ($1/\lambda^o_{2\omega} = 1/\lambda^e_\omega + 1/\lambda^e_\omega$) phase-matching conditions in the (y, z) plane at a given fundamental phase-matching wavelength λ^{PM1}_ω in a slab cut at the corresponding phase-matching angle θ_{PM1}. The corresponding effective coefficient is the following:

$$d^{GeO2}_{eff} = d_{11}(\lambda^{PM1}_{2\omega})cos^2[\theta_{PM1} - \rho^e(\theta_{PM1},\ \lambda^{PM1}_\omega)] \tag{2}$$

where ρ^e is the spatial walk-off angle at λ^{PM1}_ω and θ_{PM1}, $\lambda^{PM1}_{2\omega} = \lambda^{PM1}_\omega/2$ and d_{11} the coefficient to determine [3].

We performed a relative measurement of the magnitude of d_{11} by using KTP as a reference. Then we considered type II-SHG ($1/\lambda^o_{2\omega} = 1/\lambda^e_\omega + 1/\lambda^o_\omega$) in the (x, z) plane of KTP at a given fundamental phase-matching wavelength λ^{PM2}_ω in a slab cut at the corresponding phase-matching angle θ_{PM2}. The corresponding effective coefficient is expressed as [10]:

$$d^{KTP}_{eff} = d_{24}(\lambda^{PM2}_{2\omega})sin[\theta_{PM2} - \rho^e(\theta_{PM2},\ \lambda^{PM2}_\omega)] \tag{3}$$

were d_{24} is the excited nonlinear coefficient and ρ^e the spatial walk-off angle in the considered wavelength and direction.

Among all possibilities, we chose $\lambda^{PM1}_\omega = 1.34$ µm and $\lambda^{PM2}_\omega = 1.32$ µm in order to get rid of the setup spectral response. In this condition, the phase-matching parameters are the following: $\theta_{PM1} = 53.5°$, $\rho^e(\theta_{PM1},\ \lambda^{PM1}_\omega) = 1.07°$ for α-GeO_2 according to the present work; $\theta_{PM2} = 58.5°$, $\rho^e(\theta_{PM2},\ \lambda^{PM2}_\omega) = 2.57°$ and $d_{24}(\lambda^{PM2}_{2\omega} = 0.66\ \mu m) = 2.37\ \pm 0.17$ pm/V for KTP [9].

The fundamental wavelength was provided by a 10 ns (FWHM) and 10 Hz repetition rate pulsed Continuum OPO tunable between 0.4 µm and 2.2 µm. The fundamental beam was focused successively at normal incidence on the α-GeO_2 and KTP slabs stuck side-by-side on the same goniometric head. By using a focal length of 100 mm, we got a beam waist radius of 156 ± 5 µm inside the two crystals at λ^{PM1}_ω and λ^{PM2}_ω. The corresponding Rayleigh length is 57 ± 5 mm, which is much higher than the thicknesses of the two slabs, *i.e.*: $L_{GeO2} = 490$ µm and $L_{KTP} = 500$ µm. Thus, the propagation in the two crystals can be considered as parallel. The spatial walk-off attenuation is weak on such thin samples. However, we took it into account in the following calculations of SHG conversion efficiency in both GeO_2 and KTP crystals. The fundamental energy was controlled with an Ophir PE10 Joulemeter and set around 17 µJ to remain in the undepleted pump approximation. The Second-Harmonic (SH) generated energy was measured with an amplified photodiode Hamamatsu S2281-01 after removing the fundamental beam by using a Glan Taylor polarizer. It was necessary to add a filter and an optical density of 10^{-1} for KTP in order to remove the fundamental beam and record the SH energy ε^{KTP} of KTP with the same order of magnitude than that of α-GeO_2, *i.e.* ε^{GeO2}, due to a higher SHG conversion efficiency in KTP.

Before to describe the comparison between the two crystals, Fig. 5 shows the SH energy normalized to its maximal value. It was measured in α-GeO_2 as a function of the fundamental wavelength λ_ω around λ^{PM1}_ω.

Figure 5 shows a perfect agreement between the calculated and measured phase-matching fundamental wavelength, of α-GeO_2, *i.e.* $\lambda^{PM1}_\omega = 1.34$ µm. The measured full width of the phase-matching peak at $[sinc(\pi/2)]^2 = 0.405$ of its maximum is $\delta\lambda\omega = 93\ nm$, which is higher than the calculation using Eq. (1), *i.e.* $\delta\lambda\omega = 73\ nm$. The enlargement of the wavelength acceptance can be due to the fact that the effective interaction length is smaller than the geometric one due to some defects in the crystal. Such an agreement indicates a parallel beam propagation, which is favorable for the measurement of the nonlinear coefficient described hereafter. These conditions were also valid for the slab of KTP.

Optical Materials EXPRESS

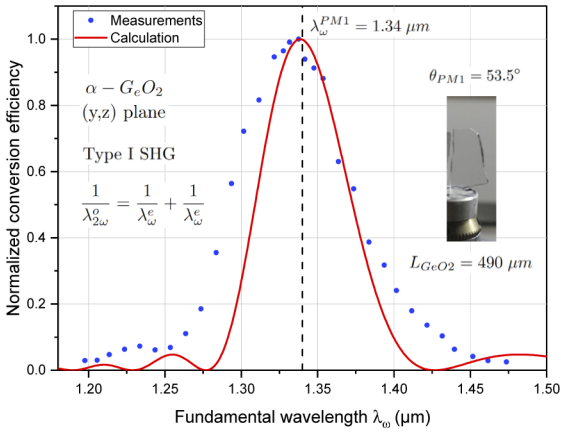

Fig. 5. Normalized Second-Harmonic energy as a function of the fundamental wavelength in the (y, z) plane of α-GeO_2. In inset a picture of the slab that was used.

The comparison between the generated SH energies ε^{GeO2} and ε^{KTP} allowed us to express the effective coefficient d_{eff}^{GeO2} as a function of d_{eff}^{KTP}, *i.e.*:

$$(d_{eff}^{GeO2})^2 = (d_{eff}^{KTP})^2 \frac{\mathcal{A}^{KTP}}{\mathcal{A}^{GeO2}} \frac{\varepsilon^{GeO2}}{\varepsilon^{KTP}} \frac{G^{KTP}}{G^{GeO2}} \frac{L_{KTP}^2}{L_{GeO2}^2} \tag{4}$$

with

$$\mathcal{A}^{GeO2} = \frac{1}{(\lambda_\omega^{PM1})^2} \frac{T_o(\lambda_{2\omega}^{PM1})}{n_o(\lambda_{2\omega}^{PM1})} \left[\frac{T_e(\theta_{PM1}, \lambda_\omega^{PM1})}{n_e(\theta_{PM1}, \lambda_\omega^{PM1})} \right]^2 \tag{5}$$

And

$$\mathcal{A}^{KTP} = \frac{1}{(\lambda_\omega^{PM2})^2} \frac{T_o(\lambda_{2\omega}^{PM2})}{n_o(\lambda_{2\omega}^{PM2})} \frac{T_o(\lambda_\omega^{PM2})}{n_o(\lambda_\omega^{PM2})} \frac{T_e(\theta_{PM2}, \lambda_\omega^{PM2})}{n_e(\theta_{PM2}, \lambda_\omega^{PM2})} \tag{6}$$

where T_o and T_e are the ordinary and extraordinary Fresnel transmission coefficients, and G the spatial walk-off attenuation [3].

Using Eq. (1) and Tab.1 for α-GeO_2 and Ref. [9] for KTP, it comes: $\mathcal{A}^{KTP} = 0.1422$, $\mathcal{A}^{GeO2} = 0.2521$, $G^{KTP} = 0.9923$ and $G^{GeO2} = 0.9995$. Then by combining Eqs. (4–6) with Eqs. (2,3), it has been possible to determine the absolute magnitude of the nonlinear coefficient of α-GeO_2, *i.e.*: $|d_{11}^{GeO2}(0.67\ \mu m)| = 0.76 \pm 0.09$ pm/V. After applying Miller's rule [10], it comes a Miller index of $\delta_{11} = 0.25$ pm/V, which leads to $|d_{11}^{GeO2}(0.532\ \mu m)| = 0.79 \pm 0.09$ pm/V. Note that it is two times smaller than the calculated value given in Ref. [4] where the wavelength dependence was not given, and three times smaller than d_{24} of KTP at 0.532 microns.

5. Conclusion

We determined the full transmission spectra in polarized light, and reported the first direct measurements of SHG, SFG and DFG phase-matching tuning curves of the positive uniaxial α-GeO_2 crystal. We also determined reliable dispersion equations for the ordinary and extraordinary principal refractive indices that are valid over the full transparency range of the crystal. From phase-matched SHG measurements, we found a nonlinear coefficient of α-GeO_2 three times smaller than that of KTP, their optical damage thresholds being comparable.

Using our dispersion equations, we found that α-GeO_2 can generate by optical parametric generation (OPG) a super continuum between 1.2 µm and 3.0 µm when pumped by a Ti:Sapphire laser at 0.86 µm and cut at $\theta = 48.3°$, as shown in Fig. 6.

All these indicators put α-GeO_2 as a new promising nonlinear crystal able to generate an optical parametric coherent radiation in the near- and mid-infrared.

Optical Materials EXPRESS

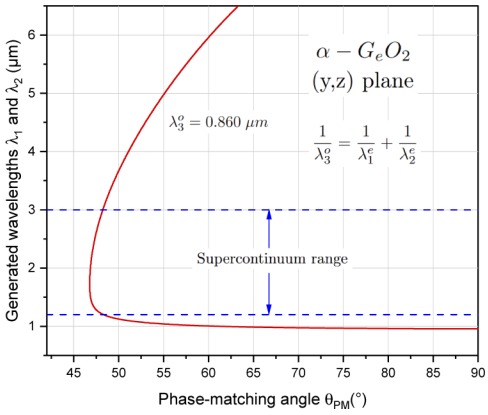

Fig. 6. Calculated super continuum by type II OPG phase-matched in the (y, z) plane of α-GeO_2 with a pump wavelength λ_3 of 0.86 µm. λ_1 and λ_2 are the wavelengths of the generated beams.

Funding. Agence Nationale de la Recherche (ANR-14-CE07-0017-1).

Disclosures. The authors declare no conflicts of interest.

Data availability. Data underlying the results presented in this paper are not publicly available at this time but may be obtained from the authors upon reasonable request.

References

1. P. Papet, M. Bah, A. Haidoux, B. Ruffle, B. Ménaert, A. Peña, J. Debray, and P. Armand, "High temperature piezoelectric properties of flux-grown α-GeO_2 single crystal," J. Appl. Phys. **126**(14), 144102 (2019).
2. G. S. Smith and P. B. Isaacs, "The crystal structure of quartz-like GeO_2," Acta Cryst. **17**(7), 842–846 (1964).
3. B. Boulanger and J. Zyss, "Nonlinear optical properties: international tables for crystallography," Vol. D, Chapter **1.7**, 178–219 (2006).
4. T. M. Glushkova, D. F. Kiselev, I. B. Makhina, M. M. Firsova, and A. P. Shtyrkova, "Trigonal germanium dioxide: Its preparation and optical parameters," Moscow Univ. Phys. Bull. **47**, 55–58 (1992).
5. A. Ligne, B. Ménaert, P. Armand, A. Peña, J. Debray, and P. Papet, "Top seeded solution growth and structural characterizations of alpha-quartz-like structure GeO_2," Cryst. Growth & Design **13**(10), 4220–4225 (2013).
6. P. Hermet, G. Fraysse, A. Lignie, P. Armand, and P. Papet, "Density functional theory predictions of the nonlinear optical properties in α-Quartz-type germanium dioxide," J. Phys. Chem. C **116**(15), 8692–8698 (2012).
7. B. Ménaert, J. Debray, J. Zaccaro, P. Segonds, and B. Boulanger, "Shaping and use of crystals as spheres and cylinders for linear and nonlinear optics," Opt. Mat. Express **7**(8), 3017–3022 (2017).
8. C. Bernerd, P. Segonds, J. Debray, T. Notake, M. Koyama, H. Minamide, and B. Boulanger, "Quadratic nonlinear optical properties of the organic N-benzyl-2-methyl-4-nitroaniline (BNA) biaxial crystal," Opt. Lett. **43**(8), 1818–1821 (2018).
9. B. Boulanger, J. P. Fève, G. Marnier, C. Bonnin, P. Villeval, and J. J. Zondy, "Absolute measurement of quadratic nonlinearities from phase-matched second-harmonic generation in a single KTP crystal cut as a sphere," J. Opt. Soc. Am. B **14**(6), 1380–1386 (1997).
10. R. C. Miller, "Optical second harmonic generation in piezoelectric crystals," Appl. Phys. Lett. **5**(1), 17–19 (1964).